26th ABCM International Congress of Mechanical Engineering
November 22-26, 2021. Florianópolis, SC, Brazil

COB-2021-0288
EVALUATING FINITE DIFFERENCE METHODS SOLVING COUPLED HEAT AND MASS TRANSFER EQUATIONS APPLIED FOR WOOD DRYING

José Henrique Kleinübing Larcher
Edgar de Oliveira Cabral Filho
Paola Buchholtz Carvalho
Viviana Cocco Mariani
Pontifical Catholic University of Paraná, PPGEM, R. Imaculada Conceição, 1155, Curitiba, Brasil.
jose.kleinubing@pucpr.edu.br; edgar.ocabral@gmail.com; pah.bcarvalho@terra.com.br; viviana.mariani@pucpr.br.

Abstract. *Wood is a multi-application material used in various industries due to its versatility, and drying is a common part of its processing. Drying can increase wood quality and dimensional stability, increasing the final value of wood products. The drying process can be described as a heat and mass transfer problem, which can result in mean temperature and moisture over time. Therefore, modeling helps to determine the necessary time for the drying procedure. Also, if the drying is poorly executed, it may damage the material, losing its commercial value. In this paper four distinct finite difference methods are used to model the wood drying diffusion process, namely, these methods are as follows: forward Euler, backward Euler, Crank-Nicolson, and Dufort-Frankel methods. These methods are applied to the process of drying Triplochiton Scleroxylon wood, also known as Ayous, a species of tree from West and Central Africa. The results from different methods are compared with experimentally obtained ones from literature. The comparison is made using the performance metrics root-mean-squared error (RMSE), mean absolute error (MAE), and the coefficient of determination (R^2). The modeling of the diffusion process is made using a pair of coupled differential equations for mass transfer and heat transfer. The overall range for moisture MAE was 3.1409-3.2703 percentage points and 0.81753-0.89104 K for temperature MAE. Results show comparable outcomes among the four methods. The implicit Euler method presents a smaller execution time. Crank-Nicolson presented the smallest MAE regarding moisture, while Dufort-Frankel and backward Euler showed the best results for temperature.*

Keywords: *wood drying, diffusion, finite difference method*

1. INTRODUCTION

Wood is a versatile material with multiple applications in industries like construction and furniture, besides its uses for heat and electrical energy production. It is widely used partially because of its availability in different places, in the form of different species. Also because of the multiple species used all over the world, its physical characteristics are hard to single out and can vary widely, as it is a biologically produced material.

Wood drying enables increased quality on wood products, preventing degradation by fungi (Kamdem *et al.*, 2002), improving the wood dimensional stability (Yang *et al.*, 2016), thus increasing its value (Jankowsky and Luiz, 2006). However, wood drying is complex a phenomenon and is hard to model. Due to its importance, several approaches have been used to model this problem. The drying models are usually divided into single board and stacked wood, with integrated models being also presented (Pang, 2007).

Herein, this paper aims to describe the heat and mass transfer in the wood drying process in wood planks from Ayous (*Triplochiton Scleroxylon*) species, through the solution of a system of coupled diffusion equations, one for each phenomenon. To achieve this, forward Euler, backward Euler, Duffort-Frankel, and Crank-Nicolson methods are used. The main contributions of this paper can be summarized as:

i Four different finite differences methods are described, which can be used for numerically solving coupled differential equations;

ii Coupled heat and mass transfer equations are used to model the wood drying process;

iii The proposed models are evaluated with different performance metrics and in computation time terms.

The remaining sections of this paper are structured as follows: Section 2 describes the heat and mass transfer model for wood drying and the experimental data used for comparison, Section 3 explains the finite difference methods utilized

in this paper, and shows the performance metrics utilized for comparison, Section 4 displays the results achieved, and in Section 5 conclusions are made and future research directions are pointed out.

2. Heat and mass transfer model

Diffusion processes can be modeled in many forms, in this section the model used in this paper-based in Simo-Tagne *et al.* (2016) is described to follow.

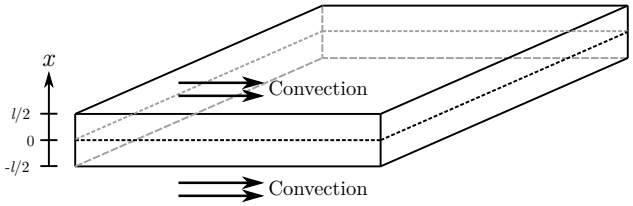

Figure 1. Schematic of the wood plank in the drying process

The drying of woods can be described by a heat and mass transfer process. On a single wood plank, the process can be presented as in Fig. 1, with the surfaces affected by convection. This process is described as a system of two coupled partial differential equations. As pointed out by Simo-Tagne *et al.* (2016), heat transfer effects can be described by Equation 1, derived from energy conservation. For these formulations the following hypotheses are taken into account (Simo-Tagne *et al.*, 2016): (i) water and air are incompressible; (ii) effects from gravity are neglected; (iii) effects from hydraulic conductivity are neglected; (iv) heat and mass transfer is neglected in the lateral faces; (v) accordingly, heat and mass transfer occurs only at the top and bottom faces of the plank; and (vi) the sample size remains constant.

$$\rho_s C_p \frac{\partial T}{\partial t} = \left[\lambda + \alpha_t \rho (E+L) D_X\right] \frac{\partial^2 T}{\partial x^2} + \rho (E+L) D_X \frac{\partial^2 X}{\partial x^2} \tag{1}$$

The boundary conditions for the heat transfer in this work's study case are (i) symmetry at the sample center, and (ii) convection at the borders. These conditions are described by Equations 2 and 3 respectively. Both these conditions are Neumann boundary conditions, as they specify the value of the first derivative.

$$\left.\frac{\partial T}{\partial x}\right)_{x=0} = 0 \tag{2}$$

$$\left.\frac{\partial T}{\partial x}\right)_{x=L/2} = \frac{h_c}{\lambda}\left(T_\infty - T\right) + \frac{\rho_s L h_m}{\lambda}\left(X_{eq} - X\right) \tag{3}$$

Similarly, the mass transfer is described by Equation 4 Simo-Tagne *et al.* (2016).

$$\frac{\partial X}{\partial t} = D_X \frac{\partial^2 X}{\partial x^2} + \alpha_t D_X \frac{\partial^2 T}{\partial x^2} \tag{4}$$

Here the boundary conditions are the same: (i) symmetry at sample center, and (ii) convection at the borders; but the equations that describe them in the mass transfer domain are Equations 5 and 6.

$$\left.\frac{\partial X}{\partial x}\right)_{x=0} = 0 \tag{5}$$

$$\left.\frac{\partial X}{\partial x}\right)_{x=L/2} = \frac{h_m}{D_X}\left(X_{eq} - X\right) \tag{6}$$

For simplicity and convenience, Equation 1 will be treated in the developments in the next sections with the following substitutions:

$$A = \left(\rho_s C_p\right), \tag{7}$$

$$B = \left[\lambda + \alpha_t \rho (E+L) D_X\right], \tag{8}$$

$$C = \left[\rho (E+L) D_X\right], \tag{9}$$

so that it can be written as

$$A\frac{\partial T}{\partial t} = B\frac{\partial^2 T}{\partial x^2} + C\frac{\partial^2 X}{\partial x^2}. \tag{10}$$

3. Numerical methods

To find the solutions for the partial differential equations that model the heat and mass transfer problem described for this work, the finite difference method was used. This method approximates the solutions employing Taylor series (Mariani *et al.*, 2008), turning the approximate solution at each time-step into a system of linear equations. For the time interpolation a forward difference is used, so that $\frac{\partial T}{\partial t} \approx \frac{T_i^{j+1} - T_i^j}{\Delta t}$, and $\frac{\partial X}{\partial t} \approx \frac{X_i^{j+1} - X_i^j}{\Delta t}$. For the approximations in space, four different schemes are used: forward Euler, backward Euler, Crank-Nicolson, and Dufort-Frankel.

3.1 Forward Euler method

The forward Euler method is also known as Euler explicit method. Figure 2a shows a stencil of which points are taken into account in a progression in time of one step. This leads to the approximations

$$\frac{\partial^2 X}{\partial x^2} \approx \frac{X_{i-1}^j - 2X_i^j + X_{i+1}^j}{\Delta x^2}, \tag{11}$$

and

$$\frac{\partial^2 T}{\partial x^2} \approx \frac{T_{i-1}^j - 2T_i^j + T_{i+1}^j}{\Delta x^2}. \tag{12}$$

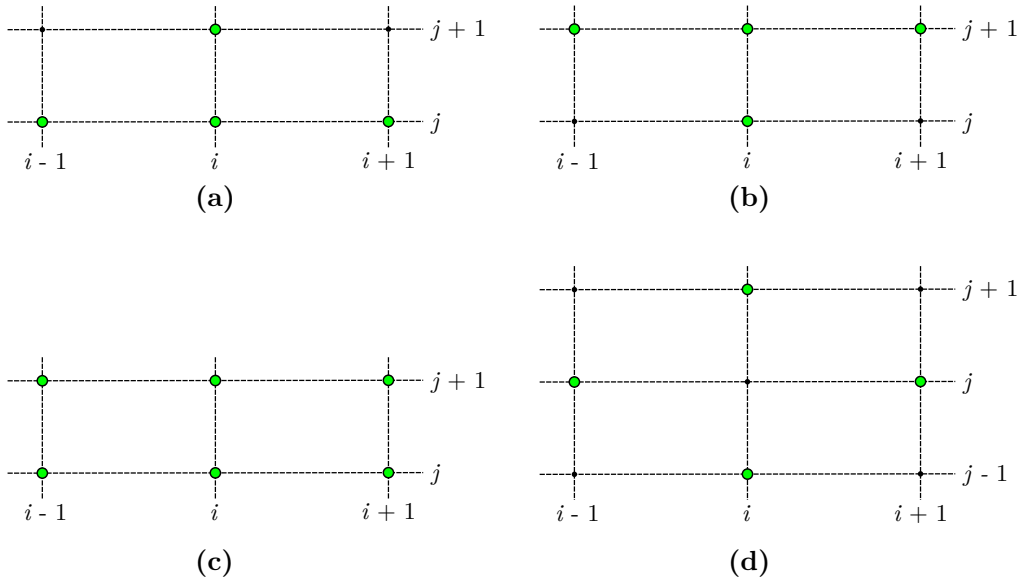

Figure 2. Stencils for (a) forward Euler, (b) backward Euler, (c) Crank-Nicolson, and (d) Dufort-Frankel methods.

Using the forward Euler scheme, Equation 1 can be discretized, with a central difference in space as follows.

$$A\frac{T_i^{j+1} - T_i^j}{\Delta t} = B\frac{T_{i-1}^j - 2T_i^j + T_{i+1}^j}{\Delta x^2} + C\frac{X_{i-1}^j - 2X_i^j + X_{i+1}^j}{\Delta x^2} \tag{13}$$

This can be simplified as:

$$T_i^{j+1} = \frac{\Delta t B}{A\Delta x^2}T_{i-1}^j + \left(1 - 2\frac{\Delta t B}{A\Delta x^2}\right)T_i^j + \frac{\Delta t B}{A\Delta x^2}T_{i+1}^j + \frac{\Delta t C}{A\Delta x^2}X_{i-1}^j - 2\frac{\Delta t C}{A\Delta x^2}X_i^j + \frac{\Delta t C}{A\Delta x^2}X_{i+1}^j. \tag{14}$$

Similarly, Equation 4 can be discretized and simplified as follows.

$$X_i^{j+1} = \frac{\Delta t D_X}{\Delta x^2}X_{i-1}^j + \left(1 - 2\frac{\Delta t D_X}{\Delta x^2}\right)X_i^j + \frac{\Delta t D_X}{\Delta x^2}X_{i+1}^j + \frac{\alpha_t \Delta t D_X}{\Delta x^2}T_{i-1}^j - 2\frac{\alpha_t \Delta t D_X}{\Delta x^2}T_i^j + \frac{\alpha_t \Delta t D_X}{\Delta x^2}T_{i+1}^j \tag{15}$$

3.2 Backward Euler method

The Forward Euler method is also known as the Euler implicit scheme. Figure 2b depicts which points are used to obtain a progression in time of Δt. In this method the approximations of the second order derivative are

$$\frac{\partial^2 T}{\partial x^2} \approx \frac{T_{i-1}^{j+1} - 2T_i^{j+1} + T_{i+1}^{j+1}}{\Delta x^2}, \tag{16}$$

and

$$\frac{\partial^2 X}{\partial x^2} \approx \frac{X_{i-1}^{j+1} - 2X_i^{j+1} + X_{i+1}^{j+1}}{\Delta x^2}. \tag{17}$$

Because the points in the next step are unknown, the values are obtained solving a system of equations, thus the method is called an implicit method. Using the backward Euler scheme, Equation 1 can be discretized, with a central difference in space as follows.

$$A\frac{T_i^{j+1} - T_i^j}{\Delta t} = B\frac{T_{i-1}^{j+1} - 2T_i^{j+1} + T_{i+1}^{j+1}}{\Delta x^2} + C\frac{X_{i-1}^{j+1} - 2X_i^{j+1} + X_{i+1}^{j+1}}{\Delta x^2} \tag{18}$$

This can be simplified as:

$$\begin{aligned} -T_i^j = +\frac{B\Delta t}{A\Delta x^2}T_{i-1}^{j+1} - \left(1 + 2\frac{B\Delta t}{A\Delta x^2}\right)T_i^{j+1} + \frac{B\Delta t}{A\Delta x^2}T_{i+1}^{j+1} \\ + \frac{C\Delta t}{A\Delta x^2}X_{i-1}^{j+1} - 2\frac{C\Delta t}{A\Delta x^2}X_i^{j+1} + \frac{C\Delta t}{A\Delta x^2}X_{i+1}^{j+1}. \end{aligned} \tag{19}$$

Similarly, Equation 4 can be discretized and simplified as follows.

$$\begin{aligned} -X_i^j = \frac{\Delta t D_X}{\Delta x^2}X_{i-1}^{j+1} - \left(1 + 2\frac{\Delta t D_X}{\Delta x^2}\right)X_i^{j+1} + \frac{\Delta t D_X}{\Delta x^2}X_{i+1}^{j+1} \\ + \frac{\alpha_t \Delta t D_X}{\Delta x^2}T_{i-1}^{j+1} - 2\frac{\alpha_t \Delta t D_X}{\Delta x^2}T_i^{j+1} + \frac{\alpha_t \Delta t D_X}{\Delta x^2}T_{i+1}^{j+1} \end{aligned} \tag{20}$$

3.3 Crank–Nicolson method

The Crank–Nicolson method is an implicit method created by Crank and Nicolson (1996), so its stencil takes the form in Figure 2c. Using the Crank-Nicolson scheme, Equation 1 can be discretized, with a central difference in space as follows.

$$\begin{aligned} A\frac{T_i^{j+1} - T_i^j}{\Delta t} = \frac{B}{2}\left(\frac{T_{i-1}^j - 2T_i^j + T_{i+1}^j}{\Delta x^2} + \frac{T_{i-1}^{j+1} - 2T_i^{j+1} + T_{i+1}^{j+1}}{\Delta x^2}\right) \\ + \frac{C}{2}\left(\frac{X_{i-1}^j - 2X_i^j + X_{i+1}^j}{\Delta x^2} + \frac{X_{i-1}^{j+1} - 2X_i^{j+1} + X_{i+1}^{j+1}}{\Delta x^2}\right) \end{aligned} \tag{21}$$

This can be simplified as

$$\begin{aligned} -A'T_{i-1}^{j+1} + (B' + 2A')T_i^{j+1} - A'T_{i+1}^{j+1} - C'X_{i-1}^{j+1} + 2C'X_i^{j+1} - C'X_{i+1}^{j+1} \\ = A'T_{i-1}^j + (B' - 2A')T_i^j + A'T_{i+1}^j + C'X_{i-1}^j - 2C'X_i^j + C'X_{i+1}^j \end{aligned} \tag{22}$$

where

$$A' = \frac{[\lambda + \alpha_t \rho (E + L) D_X]}{2\Delta x^2}, \tag{23}$$

$$B' = \frac{\rho_s C_p}{\Delta t}, \quad \text{and} \tag{24}$$

$$C' = \frac{\rho (E + L) D_X}{2\Delta x^2}. \tag{25}$$

Similarly, for mass transfer, it can be written as follows.

$$F'T_{i-1}^{j} - 2F'T_{i}^{j} + F'T_{i+1}^{j} + D'X_{i-1}^{j} + \left(E' - 2D'\right)X_{i}^{j} + D'X_{i+1}^{j} \tag{26}$$

where

$$D' = \frac{D_X}{2\Delta x^2}, \tag{27}$$

$$E' = \frac{1}{\Delta t}, \quad \text{and} \tag{28}$$

$$F' = \frac{\alpha_t D_X}{2\Delta x^2}. \tag{29}$$

3.4 Dufort-Frankel method

The Dufort-Frankel method uses an adaptation of Euler's explicit method, were using a central difference in time and substitution of T_i^j for the mean of the times $j-1$ and $j+1$. As an example, for the mass transfer, a Duffort-Frankel discretization is adapted based on Gasparin *et al.* (2018) for Equation 4. With an approximation in time in the form of $X_i^j = \frac{X_i^{j-1}+X_i^{j+1}}{2}$ and $T_i^j = \frac{T_i^{j-1}+T_i^{j+1}}{2}$, the following development yields Equation 32.

$$\frac{X_i^{j+1} - X_i^{j-1}}{2\Delta t} = D_X \frac{X_{i-1}^{j} - 2X_i^j + X_{i+1}^j}{\Delta x^2} + \alpha_t D_X \frac{T_{i-1}^{j} - 2T_i^j + T_{i+1}^j}{\Delta x^2} \tag{30}$$

$$\frac{X_i^{j+1} - X_i^{j-1}}{2\Delta t} = D_X \frac{X_{i-1}^{j} - 2\left(\frac{X_i^{j-1}+X_i^{j+1}}{2}\right) + X_{i+1}^j}{\Delta x^2} + \alpha_t D_X \frac{T_{i-1}^{j} - 2\left(\frac{T_i^{j-1}+T_i^{j+1}}{2}\right) + T_{i+1}^j}{\Delta x^2} \tag{31}$$

$$\frac{X_i^{j+1} - X_i^{j-1}}{2\Delta t} = D_X \frac{X_{i-1}^{j} - \left(X_i^{j-1} + X_i^{j+1}\right) + X_{i+1}^j}{\Delta x^2} + \alpha_t D_X \frac{T_{i-1}^{j} - \left(T_i^{j-1} + T_i^{j+1}\right) + T_{i+1}^j}{\Delta x^2}. \tag{32}$$

The stencil for the points taken in to account when the Dufort-Frankel method is used can be seen in Figure 2d. Equation 32 can be simplified as follows.

$$\left(\frac{1}{2\Delta t} + \frac{D_X}{\Delta x^2}\right)X_i^{j+1} + \frac{\alpha_t D_X}{\Delta x^2}T_i^{j+1} = \frac{D_X}{\Delta x^2}X_{i-1}^{j} + \left(\frac{1}{2\Delta t} - \frac{D_X}{\Delta x^2}\right)X_i^{j-1} + \frac{D_X}{\Delta x^2}X_{i+1}^{j} + \frac{\alpha_t D_X}{\Delta x^2}T_{i-1}^{j} - \frac{\alpha_t D_X}{\Delta x^2}T_i^{j-1} + \frac{\alpha_t D_X}{\Delta x^2}T_{i+1}^{j} \tag{33}$$

Similarly, the heat transfer equation can be discretized as follows.

$$\left(\frac{A}{2\Delta t} + \frac{B}{\Delta x^2}\right)T_i^{j+1} + \left(\frac{C}{\Delta x^2}\right)X_i^{j+1} = \left(\frac{B}{\Delta x^2}\right)T_{i-1}^{j} + \left(\frac{A}{2\Delta t} - \frac{B}{\Delta x^2}\right)T_i^{j-1} + \left(\frac{B}{\Delta x^2}\right)T_{i+1}^{j} + \left(\frac{C}{\Delta x^2}\right)X_{i-1}^{j} - \left(\frac{C}{\Delta x^2}\right)X_i^{j-1} + \left(\frac{C}{\Delta x^2}\right)X_{i+1}^{j} \tag{34}$$

According to Gasparin *et al.* (2018), the boundary condition has to be discretized using a second order of accuracy, to maintain the method features uniformly, so in this case the discretization of forward Euler method is used for boundary conditions.

3.5 Performance metrics

To evaluate the results, performance metrics are used, indicating the models deviation from the measured values or even other models. For this study the coefficient of determination (R^2), the mean absolute error (MAE), and the root mean square error (RMSE) are used. For propriety u, measured in n different points, the R^2 metric is defined by Equation 35 (Mariani *et al.*, 2008):

$$R^2 = 1 - \frac{\sum_{i=1}^{n}\left(u_i - \hat{u}_i\right)^2}{\sum_{i=1}^{n}\left(u_i - \bar{u}\right)^2}, \tag{35}$$

where u_i is the i-th known point value, $\hat{u}_i$ is the model value for the i-th point, and $\bar{u}$ is the sample mean of the n u_i values, as in equation 36.

$$\bar{u} = \frac{1}{n}\sum_{i=1}^{n} u_i \tag{36}$$

Similarly, with the same n u_i's and $\hat{u}_i$'s, the MAE is defined by Equation 37 (da Silva *et al.*, 2020). MAE can be interpreted as the average of absolute residual values.

$$\text{MAE} = \frac{1}{n}\sum_{i=1}^{n} |u_i - \hat{u}_i| \tag{37}$$

RMSE is defined by Equation 38 (Richter do Nascimento *et al.*, 2020). It can be seen as the square-root of the mean of squared errors.

$$\text{RMSE} = \sqrt{\frac{1}{n}\sum_{i=1}^{n} (u_i - \hat{u}_i)^2} \tag{38}$$

4. RESULTS

In this section, the obtained results for every approaches to solve the given problem are presented. The mesh was refined three times. The starting mesh was with $n_x = 11$. Δx can be calculated with:

$$\Delta x = \frac{L/2}{n_x - 1}. \tag{39}$$

The the mesh is refined with a ratio of 3 in Δx. Δt is calculated so the following expression remains constant.

$$\lambda \cdot \frac{\Delta t}{\Delta x^2} = \text{constant}. \tag{40}$$

So the meshes follow values at Table 1.

Table 1. Values of Δt and Δx for the simulations.

Mesh	n_x	Δx **(m)**	Δt **(s)**
Coarse	11	0.00125	2
Intermediate	33	0.000390625	0.1953125
Fine	99	0.000127551020408	0.02082465639317

The data used in this paper for comparison comes from Simo-Tagne *et al.* (2016). Moisture data is obtained experimentally using a drying chamber with controlled relative humidity for 50%. The air temperature is also controlled at 33.5°C for dry temperature and 25°C for wet temperature. 25 experimental points for the change in moisture over time are extracted from Simo-Tagne *et al.* (2016) results. Similarly, 10 points from numerical results in temperature are collected. These values are the ones used to calculate R^2, MAE and RMSE.

The numerical methods implementations were made in MATLAB R2020a running on Ubuntu 20.04.2 LTS operating system, Intel i7-5500U (4) @ 3.000GHz CPU, and NVIDIA GeForce 920M GPU.

4.1 Forward Euler

Figure 3a depicts the three different meshes and their results for moisture using the forward Euler method, while Figure 3b shows the result for temperature using the same method.

Table 2 shows the performance metrics for different values of n_x and Δt using the forward Euler method. Reducing Δt and increasing n_x in T leads to smaller MAE and RMSE, with higher values of R^2, so the simulation values get closer to the measured data points. The opposite happens to X metrics, with R^2 getting smaller and MAE and RMSE getting bigger, so further away from measured data points.

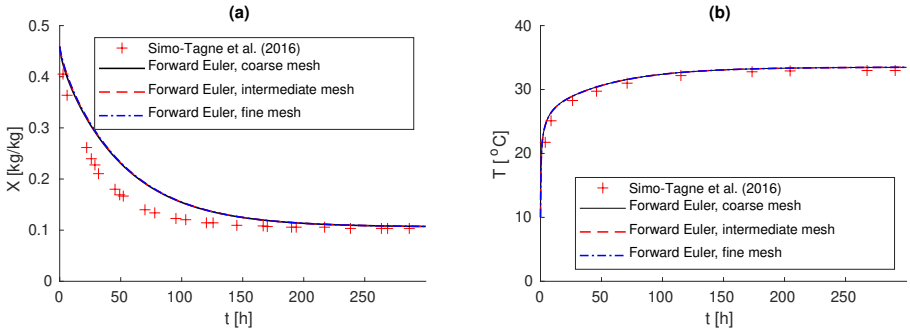

Figure 3. a) Mean moisture and b) mean temperature for different meshes using the forward Euler method

Table 2. Results for different meshes using the forward Euler method.

n_x	Δt	T			K			Execution
		R^2	MAE	RMSE	R^2	MAE	RMSE	Time (s)
11	2	0,91654	0,82788	1,0604	0,76559	3,1527	3,9178	5,7982
33	0,19531	0,91817	0,81972	1,05	0,7525	3,2428	4,0257	83,255
99	0,020825	0,91859	0,81771	1,0473	0,74842	3,2703	4,0587	1030,4135

4.2 Backward Euler

Figure 4 shows values of mean X and T for every time point using the backward Euler method.

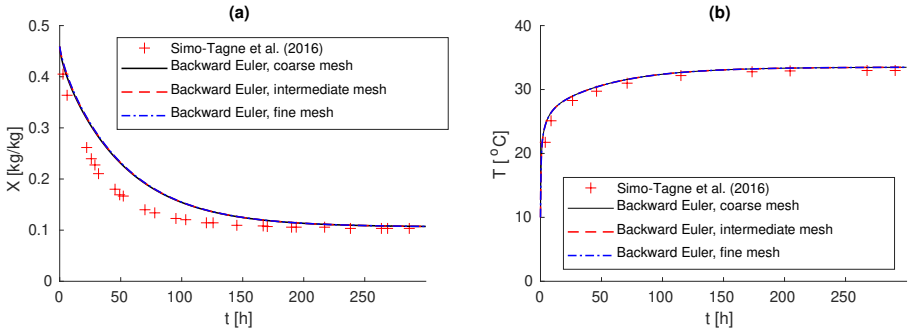

Figure 4. a) Mean moisture and b) mean temperature for different meshes using the backward Euler method

Table 3 shows results for different meshes using the backward Euler method. As with the Forward Euler method, finer meshes led to better results in T and worst results in X, regarding MAE, RMSE, and R^2. This method reduced the MAE in temperature end increased MAE regarding moisture.

Table 3. Results for different meshes using the backward Euler method.

n_x	Δt	T			X			Execution
		R^2	MAE	RMSE	R^2	MAE	RMSE	Time (s)
11	2	0,9171	0,82594	1,0568	0,76552	3,1532	3,9184	25,7898
33	0,19531	0,91833	0,81915	1,049	0,75248	3,243	4,0258	628,7871
99	0,020825	0,91865	0,81753	1,0469	0,74841	3,2703	4,0588	34307,2679

4.3 Dufort-Frankel

Figure 5 shows results using Dufort-Frankel method for the three different meshes.

Table 4 shows performance metrics values for the Dufort-Frankel method applied to solving the equations of the problem. As with the previous methods a when refining the mesh errors in X increased and errors in T decreased. This method had performance metrics very similar to the backward Euler method, with improvements in temperature and small worsen in moisture when comparing with the forward Euler method. Dufort-Frankel and backward Euler methods achieved the best results regarding temperature in all performance metrics.

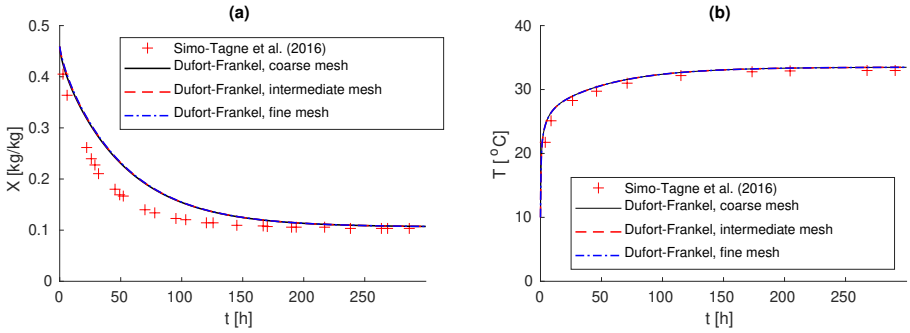

Figure 5. a) Mean moisture and b) mean temperature for different meshes using the Dufort-Frankel method

Table 4. Results for different meshes using the Dufort-Frankel method.

n_x	Δt	T			X			Execution
		R^2	MAE	RMSE	R^2	MAE	RMSE	Time (s)
11	2	0,9171	0,82594	1,0568	0,76552	3,1532	3,9184	26,7338
33	0,19531	0,91833	0,81915	1,049	0,75248	3,243	4,0258	639,3349
99	0,020825	0,91865	0,81753	1,0469	0,74841	3,2703	4,0588	33923,8087

4.4 Crank-Nicolson

For the Crank-Nicolson method, figure 6 shows how different meshes lead to close-by results.

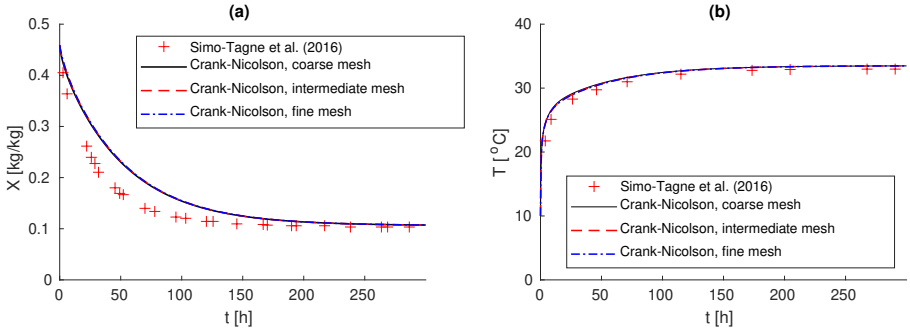

Figure 6. a) Mean moisture and b) mean temperature for different meshes using the Crank-Nicolson method

Table 5 shows the results in performance metrics for the Crank-Nicolson method with different meshes. Crank-Nicolson was the best performing scheme when moisture is taken in to account.

Table 5. Results for different meshes using the Crank-Nicolson method.

n_x	Δt	T			X			Execution
		R^2	MAE	RMSE	R^2	MAE	RMSE	Time (s)
11	2	0,90823	0,89104	1,1119	0,76713	3,1409	3,9049	28,4928
33	0,19531	0,91577	0,83939	1,0653	0,75299	3,2391	4,0217	660,2664
99	0,020825	0,91783	0,82413	1,0522	0,74858	3,2691	4,0574	33205,6956

Figure 7 compares the best mesh for each method regarding MAE, RMSE, and R^2 for moisture and temperature. All methods lead to similar results when visually compared. The fine mesh had smaller R^2 than the coarse mesh when moisture is taken into account. A reason for that can be that the used model converges to results that is offset with experimental data.

5. CONCLUSION

Four different finite difference techniques were used and evaluated with MAE, RMSE, and R^2 performance metrics. The evaluated methods were forward Euler, backward Euler, Dufort-Frankel and Crank-Nicolson. Execution time for every method was also evaluated. Computation time is tied to the number of position and time steps, but it is important to highlight that the types of operations also influence the computation time. That is why in a finer mesh, as the one with $n_x = 99$ and $\Delta t = 0,020825$, an explicit method as forwarding Euler can have execution time lower than the Crank-Nicolson, Dufort Frankel, and backwards Euler. For implicit methods a linear system is solved at every iteration, being a slower computation than simply solve basic arithmetic as in the explicit method. In this paper, all implicit methods use

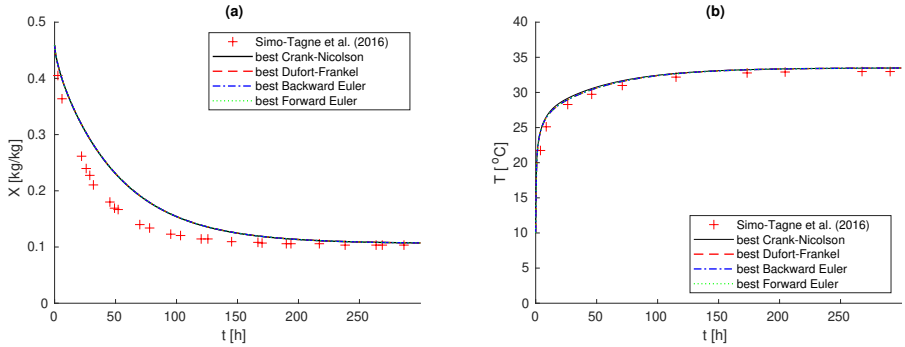

Figure 7. Best results for each method for a) moisture and b) temperature, when compared with experimental data and simulation from Simo-Tagne *et al.* (2016).

the inverse matrix method to solve for every time step, but using different methods as the Tridiagonal Matrix Algorithm (TDMA), LU factorization, and Gaussian elimination could lead to different computation times. Using the methods covered in this article, for finer meshes, it pays to use the explicit direct Euler method.

The difference in MAE, RMSE, and R^2 is relatively small when the same mesh is used. Regarding the temperature, Dufort Frankel and backward Euler gave the best results, when using the same mesh. Regarding moisture, Crank-Nicolson had the best results when using the same mesh. As the results did not exactly converge to the experimental data, it is possible in the future that a different mathematical model, proposed by Simo-Tagne (2016), for heat and mass transfer yields better results. In Mariani *et al.* (2008) a model with decoupled heat and mass equations is used and could be a good solution, so it is intended to test for future works.

For future works, it is also intended to run the tests multiple times to get average statistics of execution time. Also, it is intended to evaluate the convergence conditions for every method as in Gasparin *et al.* (2018) and compare with the obtained results.

6. ACKNOWLEDGEMENTS

The authors would like to thank the National Council of Scientific and Technologic Development of Brazil – CNPq (Grants number: 307966/2019-4-PQ), PRONEX '*Fundação Araucária*' 042/2018, and *Coordenação de Aperfeiçoamento de Pessoal de Nível Superior - Brasil* (CAPES) - Finance Code 001 for financial support of this work.

7. REFERENCES

Crank, J. and Nicolson, P., 1996. "A practical method for numerical evaluation of solutions of partial differential equations of the heat-conduction type". *Advances in Computational Mathematics*, Vol. 6, No. 1, pp. 207–226. ISSN 1572-9044. doi:10.1007/BF02127704.

da Silva, R.G., Ribeiro, M.H.D.M., Mariani, V.C. and Coelho, L.d.S., 2020. "Forecasting Brazilian and American covid-19 cases based on artificial intelligence coupled with climatic exogenous variables". *Chaos, Solitons & Fractals*, Vol. 139, p. 110027. ISSN 0960-0779. doi:10.1016/j.chaos.2020.110027.

Gasparin, S., Berger, J., Dutykh, D. and Mendes, N., 2018. "Stable explicit schemes for simulation of nonlinear moisture transfer in porous materials". *Journal of Building Performance Simulation*, Vol. 11, No. 2, pp. 129–144. ISSN 19401507. doi:10.1080/19401493.2017.1298669.

Jankowsky, I.P. and Luiz, M.G., 2006. "Review of wood drying research in Brazil: 1984–2004". *Drying Technology*, Vol. 24, No. 4, pp. 447–455. ISSN 0737-3937. doi:10.1080/07373930600611893.

Kamdem, D.P., Pizzi, A. and Jermannaud, A., 2002. "Durability of heat-treated wood". *Holz als Roh- und Werkstoff*, Vol. 60, No. 1, pp. 1–6. ISSN 1436-736X. doi:10.1007/s00107-001-0261-1.

Mariani, V.C., Barbosa de Lima, A.G. and dos Santos Coelho, L., 2008. "Apparent thermal diffusivity estimation of the banana during drying using the inverse method". *Journal of Food Engineering*, Vol. 85, No. 4, pp. 569–579. ISSN 0260-8774. doi:10.1016/j.jfoodeng.2007.08.018.

Pang, S., 2007. "Mathematical modeling of kiln drying of softwood timber: Model development, validation, and practical application". *Drying Technology*, Vol. 25, No. 3, pp. 421–431. ISSN 0737-3937. doi:10.1080/07373930601183751.

Richter do Nascimento, C.A., Mariani, V.C. and Coelho, L.d.S., 2020. "Integrative numerical modeling and thermodynamic optimal design of counter-flow plate-fin heat exchanger applying neural networks". *International Journal of Heat and Mass Transfer*, Vol. 159, p. 120097. ISSN 0017-9310. doi:10.1016/j.ijheatmasstransfer.2020.120097.

Simo-Tagne, M., Rémond, R., Rogaume, Y., Zoulalian, A. and Bonoma, B., 2016. "Modeling of coupled heat and mass transfer during drying of tropical woods". *International Journal of Thermal Sciences*, Vol. 109, pp. 299–308. ISSN

1290-0729. doi:10.1016/j.ijthermalsci.2016.06.012.

Yang, Y., Lu, J., Dong, C., Zhan, T., Jiang, J. and Luo, B., 2016. "Mathematical model of heat and moisture transfer in alder birch wood during the thermo-vacuum treatment and its application in the quantitative control of the wood color". *Drying Technology*, Vol. 34, No. 13, pp. 1567–1582. ISSN 0737-3937. doi:10.1080/07373937.2015.1137308.

8. RESPONSIBILITY NOTICE

The authors are solely responsible for the printed material included in this paper.